

Gold nanoparticles for enhanced single molecule fluorescence analysis at micromolar concentration

Deep Punj, Juan de Torres, Hervé Rigneault, and Jérôme Wenger*

CNRS, Aix Marseille Université, Centrale Marseille, Institut Fresnel, 13013 Marseille, France

* jerome.wenger@fresnel.fr

Abstract: Individual metal nanoparticles represent an inexpensive and versatile platform to enhance the detection of fluorescent species at biologically relevant concentrations. Here we use fluorescence correlation spectroscopy to quantify the near-field detection volume and average fluorescence enhancement factors set by a single gold nanoparticle. We demonstrate detection volumes down to 270 zeptoliters (three orders of magnitude beyond the diffraction barrier) together with 60-fold enhancement of the fluorescence brightness per molecule.

© 2013 Optical Society of America

OCIS codes: (240.0240) Optics at surfaces; (170.6280) Spectroscopy, fluorescence and luminescence; (350.4238) Nanophotonics and photonic crystals.

References and links

1. C. Zander, J. Enderlein, and R. A. Keller, *Single-Molecule Detection in Solution - Methods and Applications*, VCH-Wiley, Berlin/New York, 2002.
2. M. J. Levene, J. Korlach, S. W. Turner, M. Foquet, H. G. Craighead, and W. W. Webb, "Zero-mode waveguides for single-molecule analysis at high concentrations," *Science* **299**, 682–686 (2003).
3. J. Wenger, D. Gérard, J. Dintinger, O. Mahboub, N. Bonod, E. Popov, T. W. Ebbesen, and H. Rigneault, "Emission and excitation contributions to enhanced single molecule fluorescence by gold nanometric apertures," *Opt. Express* **16**, 3008–3020 (2008).
4. L. Novotny, and N. van Hulst "Antennas for light," *Nature Photon.* **5**, 83–90 (2011).
5. A. Kinkhabwala, Z. F. Yu, S. H. Fan, Y. Avlasevich, K. Mullen, and W. E. Moerner, "Large single-molecule fluorescence enhancements produced by a bowtie nanoantenna," *Nat. Photonics* **3**, 654–657 (2009).
6. E. Bermúdez Ureña, M. P. Kreuzer, S. Itzhakov, H. Rigneault, R. Quidant, D. Oron, and J. Wenger, "Excitation enhancement of a quantum dot coupled to a plasmonic antenna," *Adv. Mater.* **24**, OP314–OP320 (2012).
7. M. P. Busson, B. Rolly, B. Stout, N. Bonod, J. Wenger, and S. Bidault, "Photonic engineering of hybrid metal-organic chromophores," *Angew. Chem. Int. Ed.* **51**, 11083–11087 (2012).
8. L. C. Estrada, P. F. Aramendia and O. E. Martinez, "10000 times volume reduction for fluorescence correlation spectroscopy using nano-antennas," *Opt. Express* **16**, 20597–20602 (2008).
9. Q. Wang, G. Lu, L. Hou, T. Zhang, C. Luo, H. Yang, G. Barbillon, F. H. Lei, C. A. Marquette, P. Perriat, O. Tillement, S. Roux, Q. Ouyang, and Q. Gong, "Fluorescence correlation spectroscopy near individual gold nanoparticle," *Chem. Phys. Lett.* **503**, 256–261 (2011).
10. G. W. Lu, J. Liu, T. Y. Zhang, W. Q. Li, L. Hou, C. X. Luo, F. Lei, M. Manfait, and Q. H. Gong, "Plasmonic near-field in the vicinity of a single gold nanoparticle investigated with fluorescence correlation spectroscopy," *Nanoscale* **4**, 3359–3364 (2012).
11. H. Yuan, S. Khatua, P. Zijlstra, M. Yorulmaz, and M. Orrit, "Thousand-fold enhancement of single-molecule fluorescence near a single gold nanorod," *Angew. Chem. Int. Ed.* **125**, 1255–1259 (2013).
12. S. D. Choudhury, K. Ray, and J. R. Lakowicz, "Silver nanostructures for fluorescence correlation spectroscopy: reduced volumes and increased signal intensities," *J. Phys. Chem. Lett.* **3**, 2915–2919 (2012).
13. G. P. Acuna, F. M. Möller, P. Holzmeister, S. Beater, B. Lalkens, and P. Tinnefeld, "Fluorescence enhancement at docking sites of DNA-directed self-assembled nanoantennas," *Science* **338**, 506–510 (2012).
14. A. A. Kinkhabwala, Z. F. Yu, S. H. Fan, and W. E. Moerner, "Fluorescence correlation spectroscopy at high concentrations using gold bowtie nanoantennas," *Chem. Phys.* **406**, 3–8 (2012).

15. D. Punj, M. Mivelle, S. B. Moparthi, T. S. van Zanten, H. Rigneault, N. F. van Hulst, M. F. García-Parajó, and J. Wenger, "A plasmonic antenna-in-box platform for enhanced single-molecule analysis at micromolar concentrations," *Nature Nanotechnology* **8**, 512–516 (2013).
 16. C. Deeb, R. Bachelot, J. Plain, A.-L. Baudrion, S. Jradi, A. Bouhelier, O. Soppera, P. K. Jain, L. Huang, C. Ecoffet, L. Balan, and P. Royer, "Quantitative analysis of localized surface plasmons based on molecular probing," *ACS Nano* **4**, 4579–4586 (2010).
 17. E. Popov, M. Nevière, J. Wenger, P.-F. Lenne, H. Rigneault, P. Chaumet, N. Bonod, J. Dintinger, T. W. Ebbesen, "Field enhancement in single subwavelength apertures," *J. Opt. Soc. Am. A* **23**, 2342–2348 (2006).
 18. P. Bharadwaj, and L. Novotny, "Spectral dependence of single molecule fluorescence enhancement," *Opt. Express* **15**, 14266–14274 (2007).
 19. H. Mertens, A. F. Koenderink, and A. Polman, "Plasmon-enhanced luminescence near noble-metal nanospheres: comparison of exact theory and an improved Gersten and Nitzan model," *Phys. Rev. B* **76**, 115123 (2007).
 20. P. Bharadwaj, P. Anger, and L. Novotny, "Nanoplasmonic enhancement of single-molecule fluorescence," *Nanotechnology* **18**, 044017 (2007).
-

1. Introduction

Single molecule fluorescence studies using conventional microscopes are limited by diffraction to detection volumes in the femtoliter range. This volume dimension limits the maximum molecular concentration required to have a single molecule in the detection volume (typically in the nanomolar range), and the maximum signal-to-background ratio that can be achieved [1]. To go beyond these limits, a first approach uses circular apertures of 50 to 200 nm diameter milled in a metal film (so-called zero-mode waveguides [2]) to reduce the detection volume down to the attoliter range. However, the fluorescence signal per molecule drops dramatically as the aperture diameter is reduced below 100 nm, as a consequence of increased quenching losses [3]. To further confine the light and increase the molecular brightness, plasmonic nanoantennas stand out as powerful tools to control the light emission from nanoscale volumes [4–7]. These exciting possibilities have been applied to the detection of fluorescent molecules in solution using gold nanoparticles [8–11], silver island films [12], or more complex antenna designs [13–15].

Individual metal nanoparticles have a strong appeal for practical applications to detect fluorescent molecules in solution owing to their large availability, low intrinsic cost, and tunable spectral response. However, two technical issues are challenging the applications: (i) the large contribution in the fluorescence signal from molecules tens of nanometer away from the nanoparticles [9, 10, 12, 13] and (ii) the molecular binding to the metal [8, 11, 14]. Quantifying the near-field volume where the electric field intensity is enhanced together with the average fluorescence enhancement over this volume is of high interest [16], yet quantitative estimates for fluorescent molecules in solution are still lacking.

Here we use individual spherical gold nanoparticles to perform enhanced single molecule fluorescence analysis in solutions at high (micromolar) concentrations. Figure 1(a-c) present a schematic of the experimental configuration. Nanoparticles diameters ranging from 60 to 150 nm are used to tune the local surface plasmon resonance (LSPR) across the fluorescence excitation and emission spectra (Fig. 1(d)). At the targeted concentration of fluorescent molecules of 10 μM , the 0.5 fL confocal detection volume (diffraction-limited) contains about 3000 molecules, while only a few molecules are expected to be in the sub-attoliter near-field volume around the nanoparticle. Hence, the collected fluorescence signal is a sum of two contributions: the enhanced fluorescence from a few molecules in the nanoparticle near-field plus a fluorescence background from several thousands of freely diffusing molecules within the confocal volume. To discriminate between these contributions, we use emitters with low quantum yield and take advantage of the higher fluorescence enhancement factors obtained with them [5, 15]. We add 200 mM of methyl viologen to the solution containing the Alexa Fluor 647 dyes to quench the dye quantum yield to 8%. Lastly, to quantify the near-field detection volume and the fluorescence enhancement, we use fluorescence correlation spectroscopy (FCS)

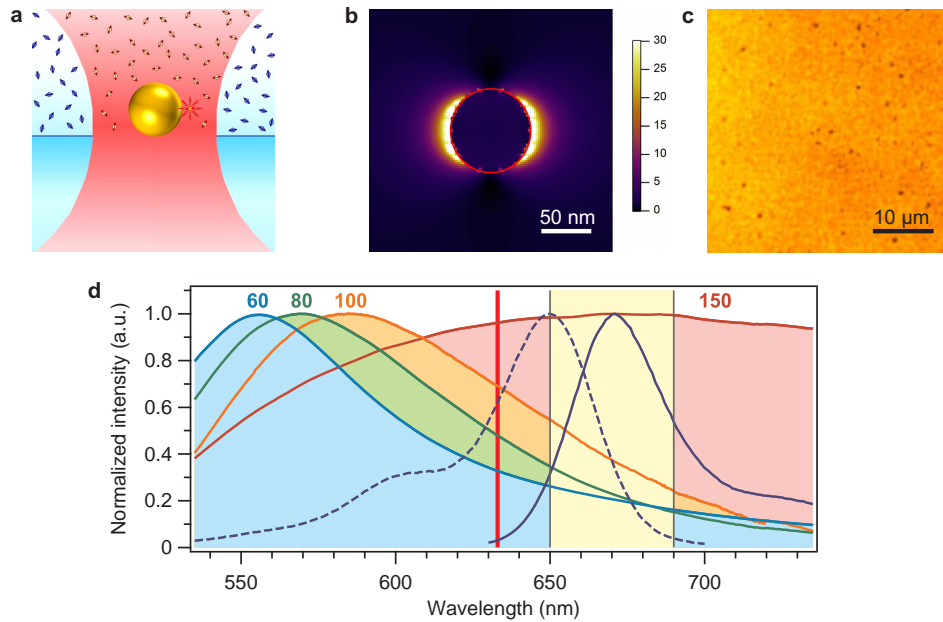


Fig. 1. (a) Gold nanoparticle on a glass substrate for enhanced single molecule analysis at high concentrations. (b) Finite-difference time-domain computation of excitation intensity enhancement near a 80 nm gold nanoparticle. The incoming light is horizontally polarized at a wavelength of 633 nm. (c) Bright-field optical image of 80 nm gold nanoparticles immobilized on a glass substrate. (d) Normalized experimental scattering cross-section of the nanoparticles (color-shaded curves, the label on top on the graphs indicates the nanoparticle diameter in nm), taken in pure water in the absence of the fluorescent species. The dashed and solid dark blue lines indicate the normalized absorption and emission spectra of Alexa Fluor 647 dye. The vertical lines indicate the 633 nm laser line used for excitation and the 650-690 nm region used for fluorescence detection.

to analyze the fluorescence trace. FCS records the temporal fluctuations of the fluorescence signal and computes its temporal correlation. For a homogeneous sample with a single fluorescent species, the amplitude of the correlation function scales with the inverse of the average number of molecules in the detection volume N . The knowledge of N together with the (calibrated) concentration of fluorescent molecules quantifies the detection volume as well as the average fluorescence brightness computed per molecule.

2. Materials and methods

Throughout this work, we use commercial gold nanoparticles (BBI Solutions) of calibrated diameters ranging from 60 to 150 nm with a typical dispersion below 10% in diameter [13]. The nanoparticles are diluted in pure water, dispersed and dried on a glass coverslip to isolate single nanoparticles, which is confirmed by confocal laser scanning and checking the invariance on the fluorescence results upon turning the linear polarization orientation of the excitation laser beam. The nanoparticle sample is covered by the solution containing Alexa Fluor 647 fluorescent dyes at micromolar concentrations together with 200 mM of methyl viologen (1,1'-Dimethyl-4,4'-bipyridinium dichloride). The experimental set-up is based on a confocal inverted microscope with a 40x 1.2NA water-immersion objective. The excitation source is a He-Ne laser at 633 nm

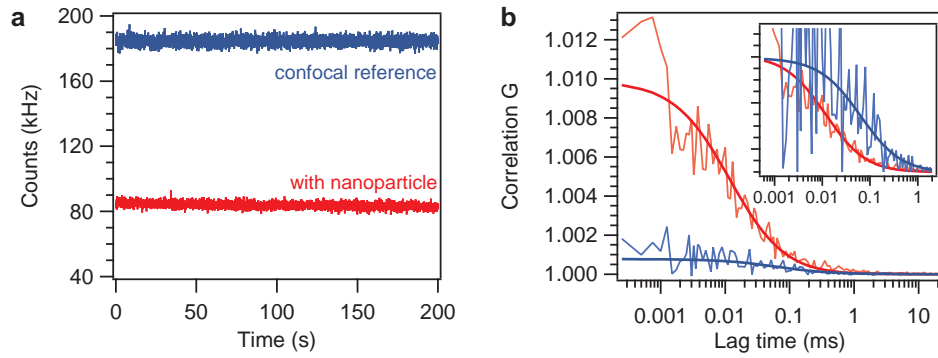


Fig. 2. (a) Fluorescence time trace and (b) FCS correlation functions for the reference confocal (blue) and the 80 nm nanoparticle (red). Alexa Fluor 647 concentration is $4.5 \mu\text{M}$, with 200 mM of methyl viologen as chemical quencher. Thick lines are numerical fit of the data using Eq. (1). The insert displays normalized FCS traces.

with $10 \mu\text{W}$ excitation power. Positioning the nanoparticle at the laser focus spot is obtained with a three-axis piezoelectric stage. A dichroic mirror and a long pass filter separate the fluorescence light from the scattered laser light. After a $30 \mu\text{m}$ confocal pinhole conjugated to the sample plane, the detection is performed by two avalanche photodiodes with $670 \pm 20 \text{ nm}$ fluorescence bandpass filters. The fluorescence intensity temporal fluctuations are analyzed with a hardware correlator (ALV6000, ALV GmbH). The analysis of the FCS data considers two species with different fluorescence brightness: N^* molecules in the nanoparticle near-field with brightness Q^* , and N_0 background molecules with brightness Q_0 diffusing away in the confocal volume. The temporal correlation G of the fluorescence intensity F can be written [1]:

$$G(\tau) = \frac{\langle F(t) \cdot F(t + \tau) \rangle}{\langle F(t) \rangle^2} = 1 + \frac{N^* Q^{*2} G_d^*(\tau) + N_0 Q_0^2 G_{d0}(\tau)}{(N^* Q^* + N_0 Q_0)^2} \quad (1)$$

where $G_d^*(\tau)$ and $G_{d0}(\tau)$ are the normalized correlation functions for each species taken individually based on a three dimensional Brownian diffusion model:

$$G_{di}(\tau) = \frac{1}{(1 + \tau/\tau_{d,i}) \sqrt{1 + s_i^2 \tau/\tau_{d,i}}} \quad (2)$$

$\tau_{d,i}$ stands for the mean residence time (set by translational diffusion) and s_i the ratio of transversal to axial dimensions of the analysis volume. Equation (1) indicates that the different fluorescent species contribute to the amplitude of G in proportion to the square of their relative fluorescence brightness. Hence, a large fluorescence enhancement in the hot spot will improve the signal-to-background contrast in the FCS curves by a quadratic manner. For the FCS analysis in the case of the nanoantenna, the number of emitters and brightness N_0 , Q_0 for the molecules diffusing away from the hot spot are fixed according to the values found at the glass-water interface without nanoparticle, corrected by a factor of $C = 1 - (d/w)^2$ to account for the screening induced by the nanoparticle (d is the nanoparticle diameter, $w=280 \text{ nm}$ is the laser beam waist at focus). Typically, C amounts to 0.95 to 0.87 for the nanoparticles of size 60 to 100 nm. In the FCS analysis, we also set $s = 0.2$, as this parameter was found to have a negligible influence on the estimates for N^* and Q^* which are the main goals of the paper.

Table 1. Fitting parameter results for the FCS curves in Fig.2(b).

	Solution reference	80nm nanoparticle
$G(0) - 1$	8×10^{-4}	9.6×10^{-3}
N	1330	0.74
Q (kHz)	0.14	8.9
τ_d (μ s)	65	11

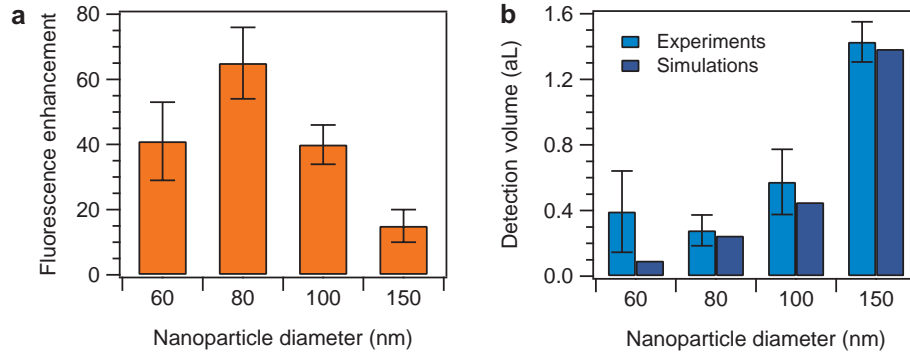


Fig. 3. Fluorescence enhancement (a) and near-field detection volume (b).

3. Experimental results

Confocal experiments on a solution at $4.5 \mu\text{M}$ fluorophore concentration yield a large fluorescence intensity with reduced temporal fluctuations (Fig. 2(a)), corresponding to a weak correlation amplitude of 8×10^{-4} (Fig. 2(b)). Fitting the confocal FCS data indicates an average number of $N_{sol} = 1330$ molecules with a diffusion time of $65 \mu\text{s}$, as expected for the 0.5 fL detection volume calibrated previously and the $4.5 \mu\text{M}$ concentration. The brightness per molecule at $10 \mu\text{W}$ excitation power with 200 mM methyl viologen is $Q_{sol} = 0.14 \text{ kHz}$. Experimental results are summarized in Tab. 1.

Performing FCS experiments with a 80 nm spherical gold nanoparticle provides correlation amplitudes about 12 times higher with significantly improved signal-to-noise ratio. FCS analysis quantifies an average number of $N^* = 0.74$ molecules in the 80 nm nanoparticle near-field with brightness $Q^* = 8.9 \text{ kHz}$. This molecular brightness corresponds to a fluorescence enhancement of $Q^*/Q_{sol} = 64$ times. Given the calibrated Alexa concentration of $4.5 \mu\text{M}$, we relate the $N^* = 0.74$ molecules in the nanoparticle near-field to a detection volume of 270 zL ($1 \text{ zL} = 10^{-21} \text{ L}$), or equivalently a detection volume reduction of $N_{sol}/N^* = 1800$ times as compared to the diffraction-limited confocal volume. Moreover, a clear reduction of diffusion time down to $11 \mu\text{s}$ is observed with the nanoparticle, which confirms that the translational diffusion events take place from a sub-diffraction volume.

FCS measurements were taken for several individual gold nanoparticles of diameter ranging from 60 to 150 nm to quantify the fluorescence enhancement factor and the near-field detection volume. The results are summarized in Fig. 3(a) and 3(b), together with estimates of the near-field detection volume derived from finite-difference time-domain simulations using the approach described in [17]. At least 10 different nanoparticles are tested for each diameter. The error bars displayed in Fig. 3 indicate the standard deviations of our measurements.

Figure 3(a) clearly indicates an optimum diameter around 80 nm for the highest fluorescence

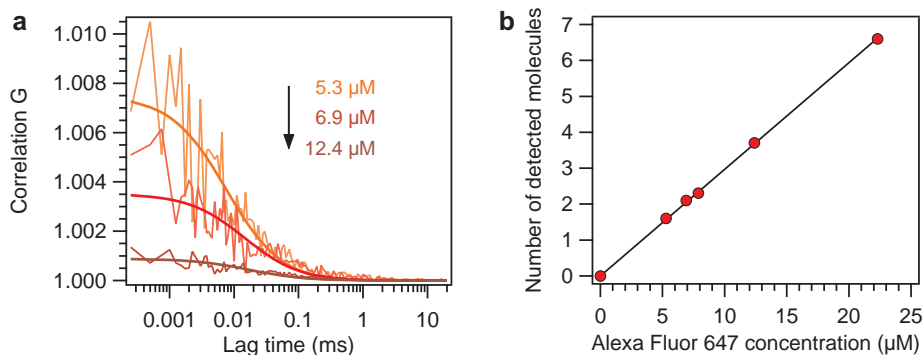


Fig. 4. (a) Fluorescence correlation functions for increasing concentrations of fluorescent probes using a 100 nm diameter gold nanoparticle. (b) Number of detected molecules in the nanoparticle near-field versus the molecular concentration.

enhancement factor. Remarkably, the 150 nm nanoparticle diameter for which the LSPR wavelength coincides with the peak fluorescence emission wavelength (Fig. 1(d)) does not provide the highest fluorescence enhancement. We find that the optimum fluorescence enhancement appears when the emission wavelength is red-shifted from the LSPR wavelength. This follows from the trade-off that must be found between radiative and non-radiative rates enhancement to achieve high fluorescence enhancement [18]. As predicted numerically [19, 20], the peak wavelength for enhanced non-radiative decay rate coincides with the LSPR wavelength but then drops rapidly towards the red side of the LSPR, while the radiative rate has a longer tail towards the red. Consequently, the quantum yield bears a more pronounced enhancement for wavelengths red-shifted as compared to the LSPR.

Lastly, series of FCS curves were recorded for increasing concentrations of fluorescent probe (Fig. 4(a)). We obtain that the number of molecules in the near-field region N^* follows a linear relationship with the fluorophore concentration (Fig. 4(b)), demonstrating that our approach can accurately quantify the number of detected molecules in the concentration regime exceeding $20 \mu\text{M}$, and provide single molecule sensitivity at relevant physiological concentrations.

4. Conclusion

Taking advantage of the 60-fold fluorescence enhancement found for low quantum yield fluorescent species near metal nanoparticles, we perform fluorescence correlation spectroscopy analysis in detection volumes down to 270 zL (three orders of magnitude beyond the diffraction barrier) within a solution of concentration exceeding ten micromolar. We provide quantitative measurements of the near-field detection volume and fluorescence enhancement factors for various sizes of gold nanoparticles. Colloidal nanoparticles represent an inexpensive and versatile platform to perform a wide variety of biochemical assays in solution with single molecule resolution at the biologically relevant micromolar concentration regime.

Acknowledgments

The research leading to these results has received funding from the European Commission's Seventh Framework Programme (FP7-ICT-2011-7) under grant 288263 NanoVista and the Agence Nationale de la Recherche under grant ANR-10-INBS-04-01 France Bio Imaging.